Active-active and active-sterile neutrino oscillation solutions to the atmospheric neutrino anomaly

M. C. Gonzalez-Garcia[1] [*], H. Nunokawa[2] [†], O. L. G. Peres[1] [‡] and
J. W. F. Valle[1] [§]

[1] *Instituto de Física Corpuscular - C.S.I.C.*

Departament de Física Teòrica, Universitat de València

46100 Burjassot, València, Spain

http://neutrinos.uv.es

[2]*Instituto de Física Gleb Wataghin, Universidade Estadual de Campinas*

13083-970 Campinas, São Paulo, Brazil

Abstract

We perform a fit to the full data set corresponding to 33.0 kt-yr of data of the Super-Kamiokande experiment as well as to all other experiments in order to compare the two most likely solutions to the atmospheric neutrino anomaly in terms of oscillations in the $\nu_\mu \to \nu_\tau$ and $\nu_\mu \to \nu_s$ channels. Using state-of-the-art atmospheric neutrino fluxes we have determined the allowed regions of oscillation parameters for both channels. We find that the Δm^2 values for the active-sterile oscillations (both for positive and negative Δm^2) are higher than for the $\nu_\mu \to \nu_\tau$ case, and that the increased Super-Kamiokande sample slightly favours $\nu_\mu \to \nu_\tau$ oscillations over oscillations into a sterile species ν_s, $\nu_\mu \to \nu_s$, and disfavours $\nu_\mu \to \nu_e$. We also give the zenith angle distributions predicted for the best fit points in each of the possible oscillation channels. Finally we compare our determinations of the atmospheric neutrino oscillation parameters with the expected sensitivities of future long-baseline experiments K2K, MINOS, ICARUS, OPERA and NOE.

14.60.Pq, 13.15.+g, 95.85.Ry

Typeset using REVTEX

---

[*]E-mail concha@evalvx.ific.uv.es

[†]E-mail nunokawa@ifi.unicamp.br

[‡]E-mail operes@flamenco.ific.uv.es

[§]E-mail valle@flamenco.ific.uv.es

I. INTRODUCTION

Atmospheric showers are initiated when primary cosmic rays hit the Earth's atmosphere. Secondary mesons produced in this collision, mostly pions and kaons, decay and give rise to electron and muon neutrino and anti-neutrinos fluxes [1]. There has been a long-standing anomaly between the predicted and observed ν_μ/ν_e ratio of the atmospheric neutrino fluxes [2]. Although the absolute individual ν_μ or ν_e fluxes are only known to within 30% accuracy, different authors agree that the ν_μ/ν_e ratio is accurate up to a 5% precision. In this resides our confidence on the atmospheric neutrino anomaly (ANA), now strengthened by the high statistics sample collected at the Super-Kamiokande experiment [4]. This experiment has marked a turning point in the significance of the ANA. The most likely solution of the ANA involves neutrino oscillations [6]. In principle we can invoke various neutrino oscillation channels, involving the conversion of ν_μ into either ν_e or ν_τ (active-active transitions) or the oscillation of ν_μ into a sterile neutrino ν_s (active-sterile transitions). Previously we have reported an exhaustive analysis of all available experimental atmospheric neutrino data for $\nu_\mu \to \nu_e$ and for $\nu_\mu \to \nu_\tau$ channels [7] but we have not discussed the sterile neutrino case. This is especially well-motivated theoretically, since it constitutes one of the simplest ways to reconcile [8–10] the ANA with other puzzles in the neutrino sector such as the solar neutrino problem [11,12] as well as the LSND result [13] and the possible need for a few eV mass neutrino as the hot dark matter in the Universe [14,15]. Although stringent limits on the existence of sterile states with large mixing to standard neutrinos have been obtained from cosmological Big-Bang Nucleosynthesis considerations [16], more conservative estimations claim that the relevant effective number of light neutrino degrees of freedom may still allow or even exceed $N_\nu = 4$ [17], thus not precluding scenarios such as given in [9]. Moreover, nucleosynthesis bounds might be evaded due to the possible suppression of active-sterile neutrino conversions in the early universe due to the presence of a lepton asymmetry that can be generated by the oscillations themselves [18].

The main aim of the present paper is to compare the $\nu_\mu \to \nu_\tau$ and the $\nu_\mu \to \nu_s$ transitions

using the the new sample corresponding to 535 days of the Super-Kamiokande data. Our present analysis uses the latest improved calculations of the atmospheric neutrino fluxes as a function of zenith angle [19], including the muon polarization effect [20] and taking into account a variable neutrino production point [21]. We determine the allowed regions for active-sterile oscillation parameters for the two possible cases $\Delta m^2 > 0$ and $\Delta m^2 < 0$. We first analyze the data using only the Super-Kamiokande results up to 535 days. Then we also perform a global analysis including the results of the Soudan2, IMB, Frejus, Nusex and Kamiokande experiments. Instead of using directly the double-ratio our analysis relies on the separate use of the electron and μ type event numbers and zenith angle distributions, with their error correlations. Following ref. [7] we explicitly check the agreement of our theoretical predictions with the experimental Monte Carlo, rendering reliability on our method.

Our main result is that the Δm^2 values for the active-sterile oscillations (both for positive and negative Δm^2) are higher than for the $\nu_\mu \to \nu_\tau$ case with maximal or nearly maximal mixing. We find that the increased Super-Kamiokande sample slightly favours $\nu_\mu \to \nu_\tau$ oscillations in comparison with $\nu_\mu \to \nu_s$, and strongly disfavours $\nu_\mu \to \nu_e$. Notice that this in contrast with our previous results in Ref. [7] were the smaller Super-Kamiokande sample did not have enought statistical weight to overcome the best fit of the $\nu_\mu \to \nu_e$ channel to the Kamiokande multi-GeV data. We find that, even though the high Super-Kamiokande statistics plays a major role in the determination of the final allowed region, there is still some appreciable weight carried by the other experiments. In the global fit case the preference for the $\nu_\mu \to \nu_\tau$ channel over the $\nu_\mu \to \nu_s$ or $\nu_\mu \to \nu_e$ channels is marginal, in clear contrast to the situation where only the Super-Kamiokande data is taken into account. Finally we compare our results of the atmospheric neutrino oscillation parameters with the accelerator neutrino oscillation searches such as CDHSW [25], CHORUS-NOMAD [26], as well as searches at reactor neutrino experiments [27–29]. We re-confirm our previous conclusions [7] that the recent data obtained at long-baseline reactor experiment CHOOZ [29] rules out at the 90 % CL the $\nu_\mu \to \nu_e$ channel as a solution to the ANA. We also compare the results of our fit with the expected sensitivities of future long-baseline experiments such as K2K [30], MINOS

[31], ICARUS [32] and NOE [33].

II. ATMOSPHERIC NEUTRINO OSCILLATION PROBABILITIES

Here we determine the expected neutrino event number both in the absence and the presence of oscillations. First we compute the expected number of μ-like and e-like events, N_α, $\alpha = \mu, e$ for each experiment

$$N_\mu = N_{\mu\mu} + N_{e\mu} , \qquad N_e = N_{ee} + N_{\mu e} , \tag{1}$$

where

$$N_{\alpha\beta} = n_t T \int \frac{d^2\Phi_\alpha}{dE_\nu d(\cos\theta_\nu)} \kappa_\alpha(h, \cos\theta_\nu, E_\nu) P_{\alpha\beta} \frac{d\sigma}{dE_\beta} \varepsilon(E_\beta) dE_\nu dE_\beta d(\cos\theta_\nu) dh . \tag{2}$$

and $P_{\alpha\beta}$ is the oscillation probability of $\nu_\alpha \to \nu_\beta$ for given values of $E_\nu, \cos\theta_\nu$ and h, i.e., $P_{\alpha\beta} \equiv P(\nu_\alpha \to \nu_\beta; E_\nu, \cos\theta_\nu, h)$. In the case of no oscillations, the only non-zero elements are the diagonal ones, i.e. $P_{\alpha\alpha} = 1$ for all α.

Here n_t is the number of targets, T is the experiment's running time, E_ν is the neutrino energy and Φ_α is the flux of atmospheric neutrinos of type $\alpha = \mu, e$; E_β is the final charged lepton energy and $\varepsilon(E_\beta)$ is the detection efficiency for such charged lepton; σ is the neutrino-nucleon interaction cross section, and θ_ν is the angle between the vertical direction and the incoming neutrinos ($\cos\theta_\nu$=1 corresponds to the down-coming neutrinos). In Eq. (2), h is the slant distance from the production point to the sea level for α-type neutrinos with energy E_ν and zenith angle θ_ν. Finally, κ_α is the slant distance distribution which is normalized to one [21].

The neutrino fluxes, in particular in the sub-GeV range, depend on the solar activity. In order to take this fact into account we use in Eq. (2) a linear combination of atmospheric neutrino fluxes Φ_α^{max} and Φ_α^{min} which correspond to the most active Sun (solar maximum) and quiet Sun (solar minimum), respectively, with different weights, depending on the running period of each experiment [7].

For definiteness we assume a two-flavour oscillation scenario, in which the ν_μ oscillates into another flavour either $\nu_\mu \to \nu_e$, $\nu_\mu \to \nu_s$ or $\nu_\mu \to \nu_\tau$. The Schröedinger evolution

equation of the $\nu_\mu - \nu_X$ (where $X = e, \tau$ or s sterile) system in the matter background for

neutrinos is given by [22]

$$i\frac{\mathrm{d}}{\mathrm{d}t}\begin{pmatrix} \nu_\mu \\ \nu_X \end{pmatrix} = \begin{pmatrix} H_\mu & H_{\mu X} \\ H_{\mu X} & H_X \end{pmatrix}\begin{pmatrix} \nu_\mu \\ \nu_X \end{pmatrix}, \tag{3}$$

$$H_\mu = V_\mu + \frac{\Delta m^2}{4E_\nu}\cos 2\theta_{\mu X}, \qquad H_X = V_X - \frac{\Delta m^2}{4E_\nu}\cos 2\theta_{\mu X},$$

$$H_{\mu X} = -\frac{\Delta m^2}{4E_\nu}\sin 2\theta_{\mu X}, \tag{4}$$

$$\tag{5}$$

where

$$V_\tau = V_\mu = \frac{\sqrt{2}G_F\rho}{M}\left(-\frac{1}{2}Y_n\right), \tag{6}$$

$$V_s = 0, \tag{7}$$

$$V_e = \frac{\sqrt{2}G_F\rho}{M}\left(Y_e - \frac{1}{2}Y_n\right) \tag{8}$$

Here G_F is the Fermi constant, ρ is the matter density at the Earth, M is the nucleon mass, and Y_e (Y_n) is the electron (neutron) fraction. We define $\Delta m^2 = m_2^2 - m_1^2$ in such a way that if $\Delta m^2 > 0\,(\Delta m^2 < 0)$ the neutrino with largest muon-like component is heavier (lighter) than the one with largest X-like component. For anti-neutrinos the signs of potentials V_X should be reversed. We have used the approximate analytic expression for the matter density profile in the Earth obtained in ref. [35]. In order to obtain the oscillation probabilities $P_{\alpha\beta}$ we have made a numerical integration of the evolution equation. The probabilities for neutrinos and anti-neutrinos are different because the reversal of sign of matter potential. Notice that for the $\nu_\mu \to \nu_\tau$ case there is no matter effect while for the $\nu_\mu \to \nu_s$ case we have two possibilities depending on the sign of Δm^2. For $\Delta m^2 > 0$ the matter effects enhance *neutrino* oscillations while depress *anti-neutrino* oscillations, whereas for the other sign ($\Delta m^2 < 0$) the opposite holds. The same occurs also for $\nu_\mu \to \nu_e$. Although in the latter case one can also have two possible signs, we have chosen the most usually assumed case where the muon neutrino is heavier than the electron neutrino, as it is theoretically more appealing. Notice also that,

5

as seen later, the allowed region for this sign is larger than for the opposite, giving the most conservative scenario when comparing with the present limits from CHOOZ.

III. ATMOSPHERIC NEUTRINO DATA FITS

Here we describe our fit method to determine the atmospheric oscillation parameters for the various possible oscillation channels, including matter effects for both $\nu_\mu \to \nu_e$ and $\nu_\mu \to \nu_s$ channels. In the latter case we consider both Δm^2 signs. Some results for the $\nu_\mu \to \nu_\tau$ and $\nu_\mu \to \nu_s$ channels have already been presented in ref. [23]. However our approach is more complete and systematic, complementing that of [23] in many ways. For example ref. [23] uses the double ratio of experimental-to-expected ratio of muon-like to electron-like events $R_{\mu/e}/R_{\mu/e}^{MC}$ and the upward-going/down-going muon ratio [24]. It is well known that the double-ratio is not well-suited from a statistical point of view due to its non-Gaussian character [38]. Although the Super-Kamiokande statistics is better, we prefer to rely on the separate use of the event numbers paying attention to the correlations between the muon predictions and electron predictions. Moreover, following ref. [7] we explicitly verify in our present reanalysis the agreement of our predictions with the experimental Monte Carlo predictions, leading to a good confidence in the reliability of our results. We also use the atmospheric neutrino flux calculation of ref. [19] instead of the Honda et al fluxes ref. [36]. Last but not least we perform a global analysis of the data, instead of focussing only on Super-Kamiokande data, admitting however the main role played by the latter experiment. In this case we take especial care in implementing the experimental detection efficiencies [37], as in ref. [7].

The steps required in order to generate the allowed regions of oscillation parameters were given in ref. [7]. As already mentioned we focus on the simplest interpretation of the ANA in terms of the neutrino oscillation hypothesis. For definiteness we assume a two-flavour oscillation scenario, in which the ν_μ oscillates into another flavour either $\nu_\mu \to \nu_e$, $\nu_\mu \to \nu_s$ or $\nu_\mu \to \nu_\tau$.

As already mentioned, when combining the results of the experiments we do not make

use of the double ratio, $R_{\mu/e}/R_{\mu/e}^{MC}$, but instead we treat the e and μ-like data separately, taking into account carefully the correlation of errors. Following ref. [7,38] we define the χ^2 as

$$\chi^2 \equiv \sum_{I,J} (N_I^{data} - N_I^{theory}) \cdot (\sigma_{data}^2 + \sigma_{theory}^2)_{IJ}^{-1} \cdot (N_J^{data} - N_J^{theory}), \tag{9}$$

where I and J stand for any combination of the experimental data set and event-type considered, i.e, $I = (A, \alpha)$ and $J = (B, \beta)$ where, A, B stands for Fréjus, Kamiokande sub-GeV, IMB,... and $\alpha, \beta = e, \mu$. In Eq. (9) N_I^{theory} is the predicted number of events calculated from Eq. (1) whereas N_I^{data} is the number of observed events. In Eq. (9) σ_{data}^2 and σ_{theory}^2 are the error matrices containing the experimental and theoretical errors respectively. They can be written as

$$\sigma_{IJ}^2 \equiv \sigma_\alpha(A) \, \rho_{\alpha\beta}(A, B) \, \sigma_\beta(B), \tag{10}$$

where $\rho_{\alpha\beta}(A, B)$ stands for the correlation between the α-like events in the A-type experiment and β-like events in B-type experiment, whereas $\sigma_\alpha(A)$ and $\sigma_\beta(B)$ are the errors for the number of α and β-like events in A and B experiments, respectively. The dimension of the error matrix varies depending on the combination of experiments included in the analysis.

We compute $\rho_{\alpha\beta}(A, B)$ as in ref. [38]. A detailed discussion of the errors and correlations used in our analysis can be found in Ref. [7]. In our present analysis, we have conservatively ascribed a 30% uncertainty to the absolute neutrino flux, in order to generously account for the spread of predictions in different neutrino flux calculations. Next we minimize the χ^2 function in Eq. (9) and determine the allowed region in the $\sin^2 2\theta - \Delta m^2$ plane, for a given confidence level, defined as,

$$\chi^2 \equiv \chi_{min}^2 + 4.61 \ (9.21) \quad \text{for} \ \ 90 \ (99)\% \ \ \text{C.L.} \tag{11}$$

There are some minor changes with respect to the assumed errors quoted in ref. [7], mainly for the Super-Kamiokande experiment. These are the following [5]:

- The error in the μ/e ratio, arising from the error in the charged current cross sections. This is estimated to be 4.3%.

- The error in the electron event number arising from the uncertainty in the neutral current cross section, which is estimated to be 3.0% (4.1%) for sub-GeV (multi-GeV) events, respectively.

- The electron versus muon mis-identification error for Super Kamiokande multi-GeV events. This is estimated to be 1.5%.

In Fig. 1 we plot the minimum value attained by the χ^2 function for fixed Δm^2 as $\sin^2 2\theta$ is varied freely, as a function of Δm^2. Notice that for large $\Delta m^2 \gtrsim 0.1$ eV^2, the χ^2 is nearly constant. This happens because in this limit the contribution of the matter potential in Eq (5) can be neglected with respect to the Δm^2 term, so that the matter effect disappears and moreover, the oscillation effect is averaged out. In fact one can see that in this range we obtain nearly the same χ^2 for the $\nu_\mu \to \nu_\tau$ and $\nu_\mu \to \nu_s$ cases. For very small $\Delta m^2 \lesssim 10^{-4}$ eV^2, the situation is opposite, namely the matter term dominates and we obtain a better fit for the $\nu_\mu \to \nu_\tau$ channel, as can be seen by comparing the $\nu_\mu \to \nu_\tau$ curve of the Super-Kamiokande sub-GeV data (dotted curve in the left panel of Fig. 1) with the solid ($\nu_\mu \to \nu_s$) and dashed ($\nu_\mu \to \nu_e$) curves in the left panel of Fig. 1). For extremely small $\Delta m^2 \lesssim 10^{-4}$ eV^2, values χ^2 is quite large and approaches a constant, independent of oscillation channel, as in the no-oscillation case. Since the average energy of Super-Kamiokande multi-GeV data is higher than the sub-GeV one, we find that the limiting Δm^2 value below which χ^2 approaches a constant is higher, as seen in the middle panel. Finally, the right panel in Fig. 1 is obtained by combining sub and multi-GeV data.

A last point worth commenting is that for the $\nu_\mu \to \nu_\tau$ case in the sub-GeV sample there are two almost degenerate values of Δm^2 for which χ^2 attains a minimum. From Fig. 1 one sees that the corresponding oscillation parameter values are $\Delta m^2 = 1.1 \times 10^{-4}$ eV^2 and 2.4×10^{-3}eV^2, both with maximal mixing. For the multi-GeV case there is just one minimum

at $1.4 \times 10^{-3} \text{eV}^2$. Finally in the third panel in Fig. 1 we can see that by combining the Super-Kamiokande sub-GeV and multi-GeV data we have a unique minimum at $1.4 \times 10^{-3} \text{eV}^2$.

IV. RESULTS FOR THE OSCILLATION PARAMETERS

The results of our χ^2 fit of the Super-Kamiokande sub-GeV and multi-GeV atmospheric neutrino data are given in Fig. 2. In this figure we give the allowed region of oscillation parameters at 90 and 99 % CL. The upper left, upper right, lower left and lower right panels show respectively the $\nu_\mu \rightarrow \nu_\tau$, $\nu_\mu \rightarrow \nu_e$ ($\Delta m^2 > 0$), $\nu_\mu \rightarrow \nu_s$ ($\Delta m^2 < 0$) and the $\nu_\mu \rightarrow \nu_s$ ($\Delta m^2 > 0$). The thick solid (thin solid) curves show the sub-GeV region at 90 (99) % CL regions and the dashed (dot-dashed) curves the multi-GeV region at 90 (99) % CL regions.

One can notice that the matter effects are similar for the upper right and lower right panels because matter effects enhance the oscillations for *neutrinos* in both cases. In contrast, in the case of $\nu_\mu \rightarrow \nu_s$ with $\Delta m^2 < 0$ the enhancement occurs only for *anti-neutrinos* while in this case the effect of matter suppresses the conversion in ν_μ's. Since the yield of atmospheric neutrinos is bigger than that of atmospheric anti-neutrinos, clearly the matter effect suppresses the overall conversion probability. Therefore we need in this case a larger value of the vacuum mixing angle, as can be seen by comparing the left and right lower panels in Fig. 2.

Notice that in all channels where matter effects play a role (all, except the upper left panel) the range of acceptable Δm^2 is shifted towards larger values, when compared with the $\nu_\mu \rightarrow \nu_\tau$ case. This follows from looking at the relation between mixing *in vacuo* and in matter [39]. In fact, whenever the magnitude of the matter potential is much larger than the difference between the two energy eigenvalues in vacuum, i.e., when $V_\mu \gg \Delta m^2/E$, there is a suppression of the mixing inside the Earth, irrespective of the sign of the matter potential and/or Δm^2. As a result, there is a lower cut in the allowed Δm^2 value, and it lies higher than what is obtained in the data fit for the $\nu_\mu \rightarrow \nu_\tau$ channel. For example, let us consider the cases of $\nu_\mu \rightarrow \nu_\tau$ and $\nu_\mu \rightarrow \nu_s$ for $\Delta m^2 > 0$. One can see comparing the upper left and lower right panels that the values of Δm^2 for $\nu_\mu \rightarrow \nu_s$ channel for the sub-GeV sample at

9

90% CL are in the range from $2.0 \times 10^{-4} \text{eV}^2$ to $7.5 \times 10^{-3} \text{eV}^2$, whereas for the $\nu_\mu \to \nu_\tau$ channel they are in the range from $5.1 \times 10^{-5} \text{eV}^2$ to $6.3 \times 10^{-3} \text{eV}^2$.

It is also interesting to analyse the effect of combining the Super-Kamiokande sub-GeV and multi-GeV atmospheric neutrino data, given in separate in Fig. 2. The results corresponding to this case are presented in Fig.3, which also indicates the best fit points. The quality of these fits can be better appreciated from Tables I and II. Comparing the values of χ^2_{min} obtained in the present work with those of ref. [7] we see that the allowed region is relatively stable with respect to the increased Super-Kamiokande statistics. However, in contrast to the case for 325.8 days, now the $\nu_\mu \to \nu_\tau$ channel is as good as the $\nu_\mu \to \nu_e$, when only the sub-GeV sample is included, with a clear Super-Kamiokande preference for the $\nu_\mu \to \nu_\tau$ channel. As before, the combined sub-GeV and multi-GeV data prefers the $\nu_\mu \to \nu_X$, where $X = \tau$ or *sterile*, over the $\nu_\mu \to \nu_e$ solution.

The zenith angle distribution changes in the presence of oscillations and it is different for each channel. The main information supportive of the oscillation hypothesis comes from the Multi-GeV muon data of Super-Kamiokande, shown in the upper right panel of Fig. 4. One can see that the zenith angle distribution of the electron data is roughly consistent with the no-oscillation hypothesis. To conclude this section we now turn to the predicted zenith angle distributions for the various oscillation channels. As an example we take the case of the Super-Kamiokande experiment and compare separately the sub-GeV and Multi-GeV data with what is predicted in the case of no-oscillation (thick solid histogram) and in all oscillation channels for the corresponding best fit points obtained for the *combined* sub and multi-GeV data analysis performed above (all other histograms). This is shown in Fig. 4. In the upper left (right) panel we show the Super-Kamiokande sub-GeV (multi-GeV) for the muon data and for zenith distributions of the muons expected for the three channels $\nu_\mu \to \nu_\tau, \nu_\mu \to \nu_e$ and $\nu_\mu \to \nu_s$. Notice that since the best fit point for $\nu_\mu \to \nu_s$ occurs at $\sin(2\theta) = 1$, the corresponding distributions are independent of the sign of Δm^2. In the lower left (right) panel of Fig. 4 we give the same information for the electron data. In the case of oscillations between two neutrino species the only relevant channel to compare to in

10

this case is the $\nu_\mu \to \nu_e$ channel.

It is worthwhile to see why the $\nu_\mu \to \nu_e$ channel is bad for the Super-Kamiokande Multi-GeV data by looking at the upper right panel in Fig. 4. Clearly the zenith distribution predicted in the no oscillation case is symmetrical in the zenith angle very much in disagreement with the data. In the presence of $\nu_\mu \to \nu_e$ oscillations the asymmetry in the distribution is much smaller than in the $\nu_\mu \to \nu_\tau$ or $\nu_\mu \to \nu_s$ channels, as seen from the figure.

V. ATMOSPHERIC VERSUS ACCELERATOR AND REACTOR EXPERIMENTS

We now turn to the comparison of the information obtained from the analysis of the atmospheric neutrino data presented above with the results from reactor and accelerator experiments as well as the sensitivities of future experiments. For this purpose we present the results obtained by combining all the experimental atmospheric neutrino data from various experiments [2,3]. In Fig. 5 we present the combined information obtained from our analysis of all atmospheric neutrino data involving vertex-contained events and compare it with the constraints from reactor experiments like Krasnoyarsk [27], Bugey [28] and CHOOZ [29], and the accelerator experiments such as CDHSW [25], CHORUS and NOMAD [26]. We also include in the same figure the sensitivities that should be attained at the future long-baseline experiments now under discussion.

The upper-left, upper-right, lower-left and lower-right panels of Fig. 5 show respectively the global fit of all atmospheric neutrino data for the $\nu_\mu \to \nu_\tau$, $\nu_\mu \to \nu_e$, $\nu_\mu \to \nu_s$ with $\Delta m^2 < 0$ and $\nu_\mu \to \nu_s$ with $\Delta m^2 > 0$. In each of these panels the star denote the best fit point of all combined data.

The first important point is that from the upper-right panel of Fig. 5 one sees that the CHOOZ reactor [29] data already exclude completely the allowed region for the $\nu_\mu \to \nu_e$ channel when all experiments are combined at 90% CL. The situation is different if only the combined sub-GeV and multi-GeV Super-Kamiokande are included. In such case the region obtained (upper-right panel of Fig. 3) is not completely excluded by CHOOZ at 90%

CL. Present accelerator experiments are not very sensitive to low Δm^2 due to their short baseline. As a result, for all channels other than $\nu_\mu \to \nu_e$ the present limits on neutrino oscillation parameters from CDHSW [25], CHORUS and NOMAD [26] are fully consistent with the region indicated by the atmospheric neutrino analysis. Future long baseline (LBL) experiments have been advocated as a way to independently check the ANA. Using different tests such long-baseline experiments now planned at KEK (K2K) [30], Fermilab (MINOS) [31] and CERN (ICARUS [32], NOE [33], and OPERA [34]) would test the pattern of neutrino oscillations well beyond the reach of present experiments. These tests are the following:

1. τ appearance searches

2. The NC/CC ratio, $\dfrac{(NC/CC)_{near}}{(NC/CC)_{far}}$. This is the most sensitive test, namely the ratio of the ratios between the total neutral current events over charged current events in a near detector over a far detector. For example the curves labelled *NC/CC ratio* at the upper-left panel of Fig. 5 delimit the sensitivity regions of these experiments with respect to this test.

3. The muon disappearance, CC_{near}/CC_{far}. This test is based on the comparison between the number of charged current interactions in a near detector and those measured in the far detector. For example, the curves labelled *Disappearance* at the lower panel of Fig. 5 delimit the sensitivity regions of the relevant experiments with respect to this test.

The second test can potentially discriminate between the active and sterile channels, i.e. $\nu_\mu \to \nu_\tau$ and $\nu_\mu \to \nu_s$. However it cannot discriminate between $\nu_\mu \to \nu_s$ and the no-oscillation hypothesis. In contrast, the last test can probe the oscillation hypothesis itself.

Notice that the sensitivity curves corresponding to the disappearance test labelled as *KEK-SK Disappearance* at the lower panels of Fig. 5 are the same for the $\nu_\mu \to \nu_\tau$ and the sterile channel since the average energy of KEK-SK is too low to produce a tau-lepton in

the far detector [1]. In contrast the MINOS experiment has a higher average initial neutrino energy and it can see the tau's. Although in this case the exclusion curves corresponding to the disappearance test are in principle different for the different oscillation channels, in practice, however, the sensitivity plot is dominated by the systematic error. As a result discriminating between $\nu_\mu \to \nu_\tau$ and $\nu_\mu \to \nu_s$ would be unlikely with the Disappearance test [42].

In summary we find that, unfortunately, the regions of oscillation parameters obtained from the analysis of the atmospheric neutrino data on vertex-contained events cannot be fully tested by the LBL experiments, when the Super-Kamiokande data are included in the fit for the $\nu_\mu \to \nu_\tau$ channel as can be seen clearly from the upper-left panel of Fig. 5. One might expect that, due to the upward shift of the Δm^2 indicated by the fit for the sterile case, it would be possible to completely cover the corresponding region of oscillation parameters. This is the case for the MINOS disappearance test. But in general since only the disappearance test can discriminate against the no-oscillation hypothesis, and this test is intrinsically weaker due to systematics, we find that also for the sterile case most of the LBL experiments can not completely probe the region of oscillation parameters indicated by the atmospheric neutrino analysis. This is so irrespective of the sign of Δm^2: the lower-left panel in Fig. 5 shows the $\nu_\mu \to \nu_s$ channel with $\Delta m^2 < 0$ while the $\nu_\mu \to \nu_s$ case with $\Delta m^2 > 0$ is shown in the lower-right panel.

VI. DISCUSSION AND CONCLUSIONS

In this paper we have compared the relative quality of the active-active and active-sterile channels as potential explanations of the ANA using the recent 535 days sample of Super-Kamiokande as well all available atmospheric neutrino data in the sub GeV and Multi GeV range (vertex-contained events). Using the most recent theoretical atmospheric neutrino

---

[1]The KEK-SK Collaboration is making a proposal of an upgrade aimed at seeing the tau's [40].

fluxes we have determined the allowed regions of oscillation parameters for $\nu_\mu \to \nu_X$ for all possible channels $X = e, \tau, s$. We find that the Δm^2 values for the active-sterile oscillations (both for positive and negative Δm^2) are higher than for the $\nu_\mu \to \nu_\tau$ case. Moreover the increased Super-Kamiokande sample slightly favours $\nu_\mu \to \nu_\tau$ oscillations in comparison to $\nu_\mu \to \nu_s$, and disfavours $\nu_\mu \to \nu_e$ more strongly. In the *global* fit of all experiments (vertex-contained events) we find a slight preference for the $\nu_\mu \to \nu_\tau$ channel over the other channels, including $\nu_\mu \to \nu_e$. Insofar as the $\nu_\mu \to \nu_e$ channel is concerned, there is no great change in the presently allowed region of all combined experiments with respect to the earlier situation: it is completely excluded by the CHOOZ experiment at the 90 %CL. What is new is that the $\nu_\mu \to \nu_e$ fit for 535 days is now worse than with the smaller sample and slightly disfavoured when in the global fit of atmospheric data *alone* and more strongly disfavoured if Super-Kamiokande data alone are combined.

We also give the zenith angle distributions predicted for the best fit points for each of the possible oscillation channel. Using the zenith angle distribution expected for multi-GeV Super-Kamiokande data in the presence of oscillation we compare the relative goodness of the three possible oscillation channels. This allows one to understand clearly why the $\nu_\mu \to \nu_\tau$ and $\nu_\mu \to \nu_s$ channels are much better than the $\nu_\mu \to \nu_e$ channel which is in any case ruled out by CHOOZ. The main support for the ν_μ to ν_τ oscillation hypothesis comes from the Super-Kamiokande Multi-GeV muon data.

Finally we compare our determinations of the atmospheric neutrino oscillation parameters with the expected sensitivities of future long-baseline experiments such as K2K, MINOS, ICARUS, NOE and OPERA. We have found that, unfortunately, the regions of oscillation parameters obtained from the analysis of the atmospheric neutrino data on vertex-contained events cannot be fully probed by most of the LBL experiments. Despite the Δm^2 values indicated by the atmospheric data for the sterile case are higher than for the $\nu_\mu \to \nu_\tau$ channel, the need to rely on the disappearance test makes it difficult to completely test the region of atmospheric neutrino oscillation parameters at the presently proposed LBL experiments. From this point of view a re-design of such experiments would be desirable, as recently

suggested by NOE [41].

REFERENCES

[1] For reviews, see for e.g., T.K. Gaisser, in Neutrino '96, Proc. of the 17th International Conference on Neutrino Physics and Astrophysics, Helsinki, Finland, edited by K. Enquist, K. Huitu and J. Maalampi (World Scientific, 1997), p. 211; T.K. Gaisser, F. Halzen and T. Stanev, Phys. Rep. 258, 174 (1995); T. Stanev, Proceedings of TAUP95, Toledo, Spain, edited by A. Morales, J. Morales and J. A. Villar [Nucl. Phys. B (Proc. Suppl.) **48** 165 (1996)]; T. Kajita, in *Physics and Astrophysics of Neutrinos*, ed. by M. Fukugita and A. Suzuki (Springer-Verlag,Tokyo, 1994), p. 559; E. Kh. Akhmedov, in *Cosmological Dark Matter*, Proceedings of the International School on Cosmological Dark Matter, Valencia, ed. A. Perez and J.W.F.Valle (World Scientific, Singapore, 1994, ISBN 981-02-1879-6), p. 131.

[2] IMB Collaboration, D. Casper *et al.*, Phys. Rev. Lett. **66**, 2561 (1991); R. Becker-Szendy *et al.*, Phys. Rev. **D46**, 3720 (1992); Kamiokande Collaboration, H. S. Hirata *et al.*, Phys. Lett. **B205**, 416 (1988) and Phys. Lett. **B280**, 146 (1992); Kamiokande Collaboration, Y. Fukuda *et al.*, Phys. Lett. **B335**, 237 (1994); Soudan Collaboration, W. W. M Allison *et al.*, Phys. Lett. **B391**, 491 (1997); Soudan Collaboration, T. Kafka *et al.*, talk given TAUP97, September 7-11, 1997 - Laboratori Nazionali del Gran Sasso, Assergi, Italy, hep/ph 9712281.

[3] NUSEX Collaboration, M. Aglietta *et al.*, Europhys. Lett. **8**, 611 (1989); Fréjus Collaboration, Ch. Berger *et al.*, Phys. Lett. **B227**, 489 (1989)

[4] Super-Kamiokande Collaboration: Y. Fukuda et al, hep-ex/9805006; Super-Kamiokande Collaboration: Y. Fukuda et al, hep-ex/9803006

[5] Super-Kamiokande Collaboration, E. Kearns *et al.*, talk given at TAUP97, Laboratori Nazionali del Gran Sasso, Assergi, Italy, 1997, hep-ex/9803007. Ed. Kearns , private communication.

[6] J. G. Learned, S. Pakvasa, and T. J. Weiler, Phys. Lett. **B207**, 79 (1988); V. Barger and K. Whisnant, Phys. Lett. **B209**, 365 (1988); K. Hidaka, M. Honda, and S. Midorikawa,

Phys. Rev. Lett. **61**, 1537 (1988).

[7] M. C. Gonzalez-Garcia, H. Nunokawa, O. L. G. Peres, T. Stanev and J. W. F. Valle, Phys. Rev. **D58**, 033004 (1998) and references therein.

[8] For a review see, J. W.F. Valle, in Proceedings of Workshop *Beyond the Desert 1997: Accelerator and Nonaccelerator Approaches*, Tegernsee, Germany, 8-14 Jun 1997, ed. H. V. Klapdor and H. Pas (Inst. of Physics, 1998), e-Print Archive: hep-ph/9712277.

[9] J. T. Peltoniemi, D. Tommasini, and J. W. F. Valle, Phys. Lett. **B298**, 383 (1993); A. Joshipura, A. Yu. Smirnov, hep-ph/9806376

[10] J. T. Peltoniemi and J. W. F. Valle, Nucl. Phys. **B406**, 409 (1993); D. Caldwell and R. N. Mohapatra, Phys. Rev. **D50**, 3477 (1994); G. M. Fuller, J. R. Primack and Y.-Z. Qian, Phys. Rev. **D52**, 1288 (1995); J. J. Gomez-Cadenas and M. C. Gonzalez-Garcia, Zeit. fur Physik **C71**, 443 (1996); E. Ma and P. Roy, Phys. Rev. **D52**, R4780 (1995); E. Ma and J. Pantaleone, Phys. Rev. **D52**, R3763 (1995); R. Foot and R. R. Volkas, Phys. Rev. **D52**, 6595 (1995): Z. G. Berezhiani and R. N. Mohapatra, Phys. Rev. **D52**, 6607 (1995); E. J. Chun, A. S. Joshipura and A. Y. Smirnov, Phys. Lett. **B357**, 608 (1995); Q. Y. Liu and A. Yu. Smirnov, hep-ph/9712493; V. Barger, K. Whisnant and T. Weiler, Phys. Lett. **B427**, 97 (1998); S. C. Gibbons, R. N. Mohapatra, S. Nandi and A. Raychaudhuri, Phys. Lett. **B430**, 296 (1998); V. Barger, S. Pakvasa, T. J. Weiler, K. Whisnant, hep-ph/9806328.

[11] Kamiokande Collaboration, Y. Fukuda *et al.*, Phys. Rev. Lett. **77**, 1683(1996); Gallex Collaboration: P. Anselmann *et al.*, Phys. Lett. B**342**, 440 (1995) and W. Hampel *et al.*, Phys. Lett. B**388**, 364 (1996); Sage Collaboration, V. Gavrin *et al.*, in Neutrino *'96*, Proceedings of the 17th International Conference on Neutrino Physics and Astrophysics, Helsinki, edited by K. Huitu, K. Enqvist and J. Maalampi (World Scientific, Singapore, 1997), p. 14; Super-Kamiokande Collaboration: R. Svoboda *et al.*, ITP Conference on Solar Neutrinos: News About SNUs, December 2-6, 1997, http://www.itp.ucsb.edu/online/snu/svoboda/ and H. Sobel, Aspen Winter Conference on Particle Physics, January 25-31, 1998,

http://www.physics.arizona.edu/ina/aspen98.html.

[12] J. N. Bahcall, S. Babu and M. H. Pisonneault, Phys. Lett. **B433**, 1 (1998); J. N. Bahcall, P. I. Krastev, A. Yu. Smirnov, hep-ph/9807216

[13] C. Athanassopoulos, Phys. Rev. Lett. **77**, 3082 (1996); Phys. Rev. **C54**, 2708 (1996); J. E. Hill, Phys. Rev. Lett. **75**, 2654 (1995).

[14] R. Shaefer and Q. Shafi, *Nature* **359**, 199 (1992); E. L. Wright *et al.*, Astrophys. J. **396**, L13 (1992); A. Klypin *et al.*, ibid. **416**, 1 (1993);

[15] J. R. Primack *et al.*, Phys. Rev. Lett. **74**, 2160 (1995).

[16] D. Schramm and M. Turner, Rev. Mod. Phys. **70**, 303 (1998)

[17] P. J. Kernan and S. Sarkar, *Phys. Rev.* **D 54** (1996) 3681; S. Sarkar, *Reports on Progress in Physics* **59** (1996) 1

[18] R. Foot and R. Volkas, Phys. Rev. **D55**, 5147; Phys. Rev. **D56**, 6653 (1997).

[19] V. Agrawal *et al.*, Phys. Rev. **D53**, 1314 (1996) and *An Improved Calculation of the Atmospheric Neutrino Flux*, T.K.Gaisser and T.Stanev, in Proceedings of the 24th ICRC, Rome, 1995, edited by B. D'Ettore Piazzoli *et al.*, Rome, Italy, 1995, Vol. 1, p. 694.

[20] L. V. Volkova, Sov. J. Nucl. Phys. **31**, 784 (1980).

[21] T. K. Gaisser and T. Stanev, Phys. Rev. **D57** 1977 (1998).

[22] L. Wolfenstein, Phys. Rev. **D17**, 2369 (1985); V. Barger et al., Phys. Rev. **D22**, 2718 (1981); P. Langacker et al., Phys. Rev. **D27**, 1228 (1983); V. Barger et al., Phys. Rev. **D43**, 1759 (1991).

[23] R. Foot, R. R. Volkas and O. Yasuda, Phys. Rev. **D58**, 013006 (1998); Phys. Lett. **B421**, 245 (1998); O. Yasuda, hep-ph/9809206.

[24] J. W. Flanagan, J. G. Learned and S. Pakvasa, Phys. Rev. **D57**, 2649 (1998).

[25] CDHSW Collaboration, F. Dydak *et al.*, Phys. Lett. **B134**, 281 (1984).

[26] CHORUS Collaboration, E. Eskut *et al.*, Nucl. Instrum. Meth. A **401**, 7 (1997); NOMAD Collaboration, J. Altegoer *et al.*, Nucl. Instrum. Meth. A **404**, 96 (1998). L. Di Lella *et al.*, talk given at TAUP97, Laboratori Nazionali del Gran Sasso, Assergi, Italy,

1997.

[27] G. S. Vidyakin *et al.*, JETP Lett. **59**, 390 (1994).

[28] B. Achkar *et al.*, Nucl. Phys. **B424**, 503 (1995).

[29] CHOOZ Collaboration, M. Apollonio *et al.*, Phys. Lett. B **420** 397(1998).

[30] KEK-SK Collaboration, C. Yanagisawa, talk at International Workshop on Physics Beyond The Standard Model: from Theory to Experiment, Valencia, Spain, October 13-17, 1997, to appear in the proceedings, ed. by I. Antoniadis, L. Ibanez and J. W. F. Valle (World Scientific, 1998); KEK-SK Collaboration,*Proposal for Participation in Long-Baseline Neutrino Oscillation Experiment E362 at KEK*, W. Gajewski *et al.* (unpublished).

[31] MINOS Collaboration, D. Michael *et al.*, Proceedings of *XVI International Workshop on Weak Interactions and Neutrinos*, Capri, Italy, 1997, edited by G. Fiorilo *et al.*, [Nucl. Phys. B (Proc. Suppl.)**66** (1998) 432].

[32] ICARUS Collaboration, A. Rubia *et al.*, Proceedings of *XVI International Workshop on Weak Interactions and Neutrinos*, Capri, Italy, 1997, edited by G. Fiorilo *et al.*, [Nucl. Phys. B (Proc. Suppl.) **66** (1998) 436].

[33] NOE Collaboration, M. Ambrosio *et al.*, Nucl. Instr. Meth. A**363**, 604 (1995); NOE Proposal, *NOE Detector for the long baseline neutrino oscillation experiment*, available at the homepage http://www.na.infn.it/SubNucl/accel/noe/noe.html

[34] OPERA Collaboration, A. Ereditato *et al.*, Proceedings of *XVI International Workshop on Weak Interactions and Neutrinos*, Capri, Italy, 1997, edited by G. Fiorilo *et al.*, [Nucl. Phys. B (Proc. Suppl.) **66** (1998) 423].

[35] E. Lisi and D. Montanino, Phys. Rev. **D56**, 1792 (1997).

[36] M. Honda, T. Kajita, S. Midorikawa and K. Kasahara, Phys. Rev. **D52**, 4985 (1995).

[37] K. Inoue, private communication.

[38] G. L. Fogli, E. Lisi, Phys. Rev. **D52**, 2775 (1995); G. L. Fogli, E. Lisi and D. Montanino, Phys. Rev. **D49**, 3626 (1994); Astrop. Phys. **4**, 177 (1995); G. L. Fogli, E. Lisi, D. Montanino and G. Scioscia Phys. Rev. **D55**, 485 (1997).

[39] S. P. Mikheyev and A. Yu. Smirnov, Yad. Fiz. **42**, 1441 (1985); L. Wolfenstein, Phys. Rev. **D17**, 2369 (1985).

[40] C. Yanagisawa, private communication.

[41] After the completion of ref. [7], the NOE Collaboration has proposed a redesign of the experiment. We show the updated figure from [33].

[42] M. Goodman, private communication.

Experiment		$\nu_\mu \to \nu_\tau$	$\nu_\mu \to \nu_s$	$\nu_\mu \to \nu_e$
Super-Kam sub-GeV	χ^2_{min}	6.1	7.7	7.3
	Δm^2 (10^{-3}eV^2)	0.11	1.6	1.2
	$\sin^2 2\theta$	1.0	1.0	0.97
Super-Kam multi-GeV	χ^2_{min}	6.3	7.9	10.8
	Δm^2 (10^{-3}eV^2)	1.4	3.5	25.4
	$\sin^2 2\theta$	0.97	1.0	0.74

TABLE I. Minimum value of χ^2 and the best fit point for Super-Kamiokande sub-GeV and Multi-Gev data and for each oscillation channel. Notice that for $\nu_\mu \to \nu_s$ the minimum χ^2 is practically independent of the sign of Δm^2 as the minimum is located at maximum mixing angle.

Experiment		$\nu_\mu \to \nu_\tau$	$\nu_\mu \to \nu_s$	$\nu_\mu \to \nu_e$	
Super-Kam Combined	χ^2_{min}	13.7	16.5	21.9	
	Δm^2 (10^{-3}eV^2)	1.4	2.2	1.4	
	$\sin^2 2\theta$	1.0	1.0	0.96	
All experiments Combined	χ^2_{min}	49.5	50.8	50.8	
	Δm^2 (10^{-3}eV^2)	3.0	3.3	3.0	
	$\sin^2 2\theta$	1.0	1.0	0.99	

TABLE II. Minimum value of χ^2 from for the combined data of Super-Kamiokande only (upper part of table) and for all experiments (lower part of table) and the best fit point for each type of oscillation channels.
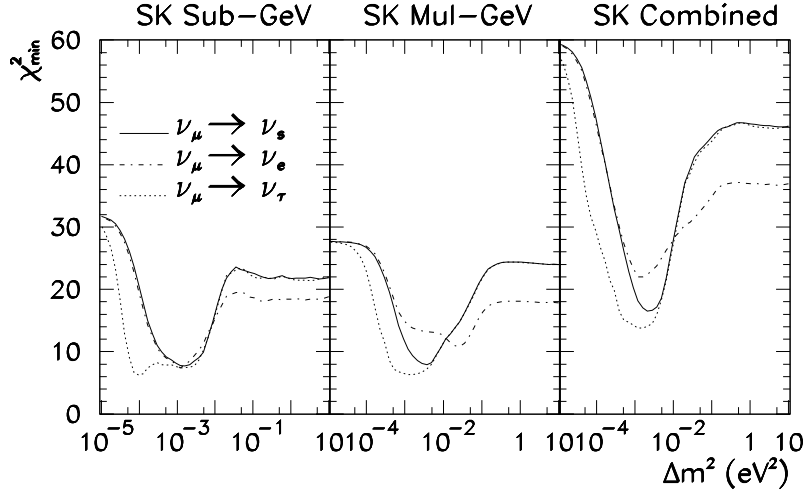
FIG. 1. χ^2_{min} for fixed Δm^2 versus Δm^2 for each oscillation channel for Super-Kamiokande sub-GeV and multi-GeV data, and for the combined sample. Since the minimum is always obtained close to maximum mixing the curves for $\nu_\mu \to \nu_s$ for both signs of Δm^2 coincide.
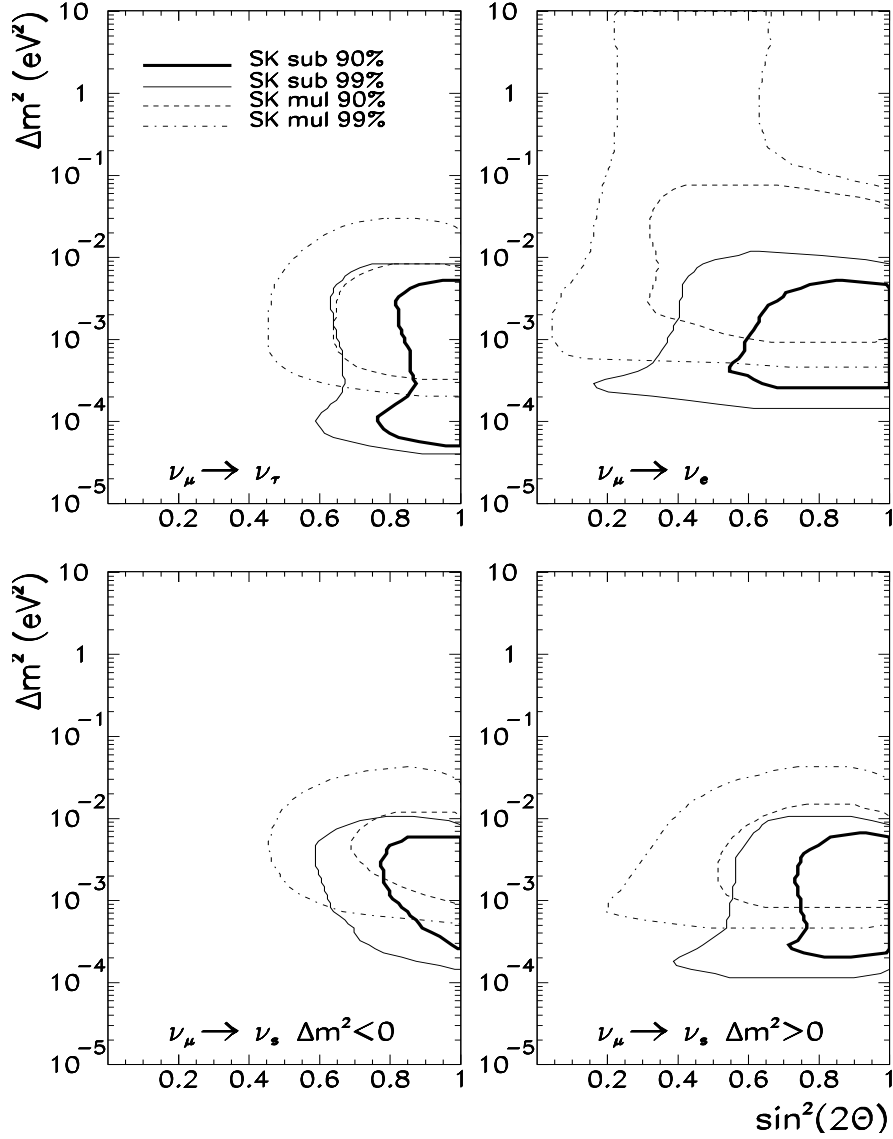
FIG. 2.   Allowed regions of oscillation parameters for Super-Kamiokande for the different oscillation channels as labeled in the figure. In each panel, we show the allowed regions for the sub-GeV data at 90 (thick solid line) and 99 % CL (thin solid line) and the multi-GeV data at 90 (dashed line) and 99 % CL (dot-dashed line).
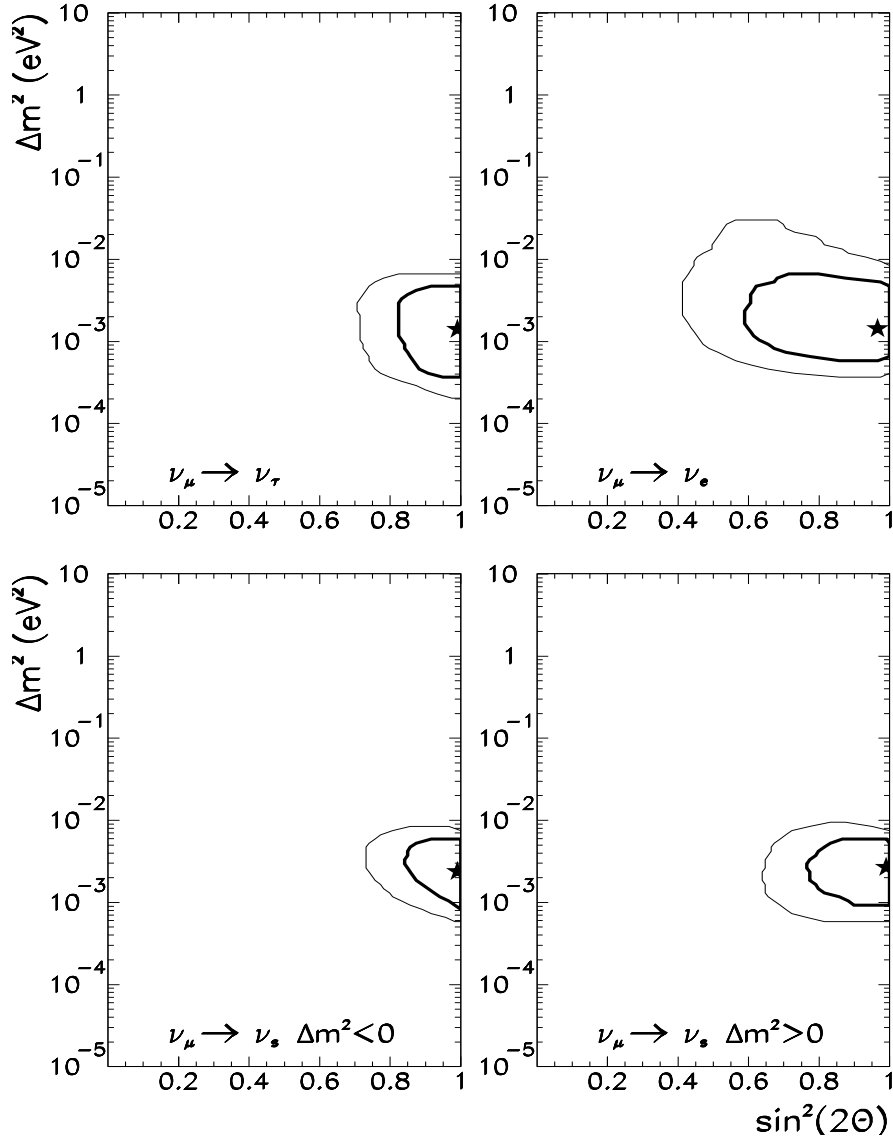
FIG. 3. Allowed oscillation parameters of Super-Kamiokande data combined at 90 (thick solid line) and 99 % CL (thin solid line) for the different oscillation channels as labeled in the figure. In each panel the best fit point is marked by a star.
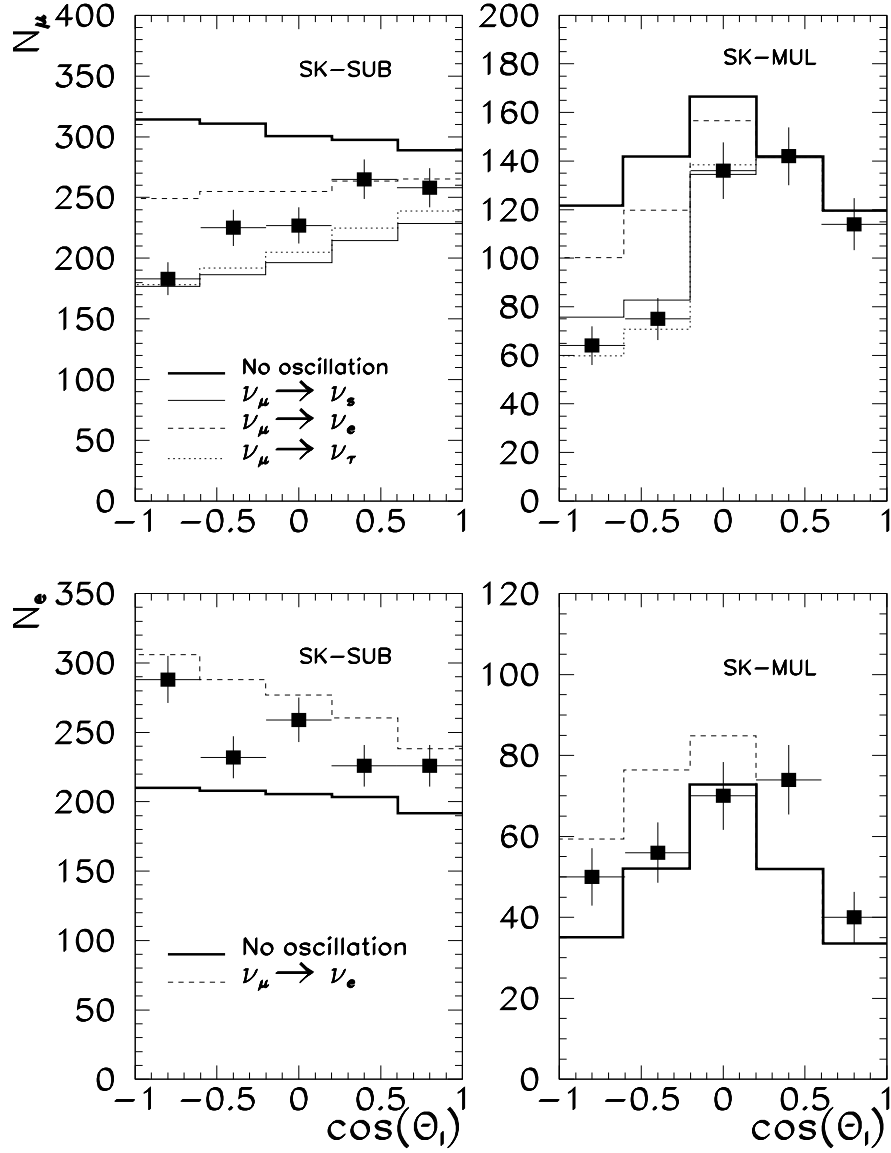
FIG. 4. Angular distribution for Super-Kamiokande electron-like and muon- like sub-GeV and multi-GeV events, together with our prediction in the absence of oscillation (thick solid line) as well as the predictions for the best fit points in each oscillation channel: $\nu_\mu \to \nu_s$ (thin solid line), $\nu_\mu \to \nu_e$ (dashed line) and $\nu_\mu \to \nu_\tau$ (dotted line). The errors displayed in the experimental points is only statistical.
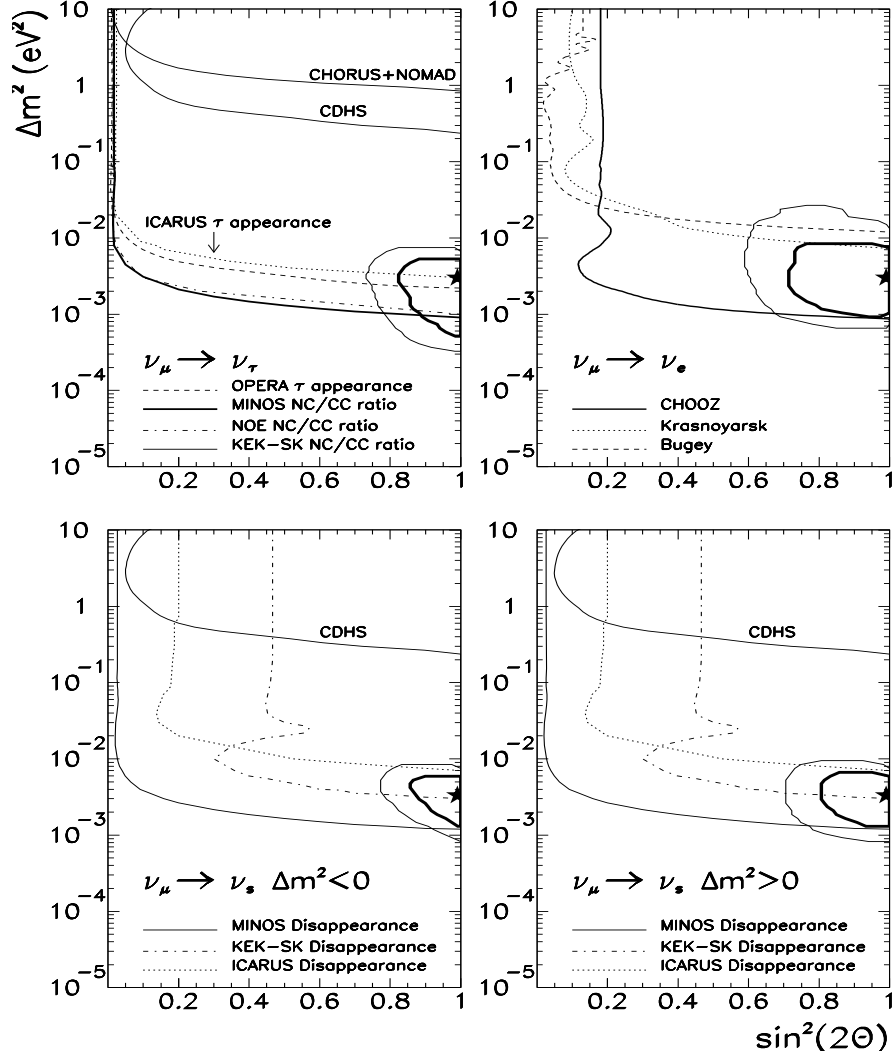
25

FIG. 5. Allowed oscillation parameters for all experiments combined at 90 (thick solid line) and 99 % CL (thin solid line) for each oscillation channel as labeled in the figure. We also display the expected sensitivity of the future long-baseline experiments in each channel: MINOS, KEK-SK, NOE, ICARUS and OPERA, as well as the present constraints of accelerator and reactor experiments: CHOOZ, Bugey and Krasnoyarsk for the $\nu_\mu \to \nu_e$ channel, CDHSW and CHORUS (NOMAD) for $\nu_\mu \to \nu_x$, where $x = \tau$ or sterile. The best fit point is marked with a star.